



# Late Neogene terrestrial climate reconstruction of the central Namib Desert derived by the combination of U–Pb silcrete and terrestrial cosmogenic nuclide exposure dating

Benedikt Ritter<sup>1,★</sup>, Richard Albert<sup>2,3,★</sup>, Aleksandr Rakipov<sup>2,3</sup>, Frederik M. Van der Wateren<sup>4</sup>, Tibor J. Dunai<sup>1</sup>, and Axel Gerdes<sup>2,3</sup>

<sup>1</sup>Institute of Geology & Mineralogy, University of Cologne, Cologne, Germany

<sup>2</sup>Frankfurt Isotope and Element Research Center (FIERCE), Goethe University Frankfurt, Frankfurt, Germany

<sup>3</sup>Institute of Geosciences, Goethe University Frankfurt, Frankfurt, Germany

<sup>4</sup>Philosophical Practice, Cas Oorthuyskade 23, 1087 DP Amsterdam, the Netherlands

★These authors contributed equally to this work.

**Correspondence:** Benedikt Ritter (benedikt.ritter@uni-koeln.de) and Richard Albert (albertroper@em.uni-frankfurt.de)

Received: 27 June 2023 – Discussion started: 6 July 2023

Revised: 22 September 2023 – Accepted: 9 October 2023 – Published: 1 December 2023

**Abstract.** The chronology of the Cenozoic “Namib Group” of the Namib Desert is rather poorly understood and lacks direct radiometric dating. Thus, the paleoclimate and landscape evolution of the central Namib Desert remains imprecise, complicating the detailed search for global and/or local forcing factors for the aridification of the Namib. The widespread occurrence of calcretes and silcretes in the Namib Desert allows us to apply the novel application of the U–Pb laser ablation dating technique on silcretes and calcretes to date important phases of landscape stability and to retrieve critical paleoclimatic and environmental information on desertification and its paleoclimatic variability. Microscale silcrete formation (maximum of 8 mm) due to pressure solution by expanding calcrete cementation provides the opportunity to date multiple phases (multiple generations of silcrete as growing layers or shells) of silcrete formation. Groundwater silcrete and calcrete formation occurred at our study site during the Pliocene, a period of relatively stable climate and landscape conditions under semi-arid to arid conditions. Terrestrial cosmogenic nuclide (TCN) exposure ages from flat canyon rim surfaces indicate the cessation of groundwater calcrete formation due to incision during the Late Pliocene–Early Pleistocene and mark a large-scale landscape rejuvenation due to climate shifts towards more arid conditions in the Pleistocene, which can be connected to global climate patterns. This study demonstrates the feasibility of applying U–Pb

laser ablation to groundwater silcrete and calcretes, discusses several important issues associated with this technique, and opens up the possibility of dating numerous sedimentary sequences containing silcretes and calcretes in arid environments. In particular, the use of silcretes (as described above) reduces potential effects of detrital components and bulk signal measurements by using massive calcretes. Our study redefines and improves the generally accepted Late Cenozoic chronostratigraphy of the Namib Desert (Miller, 2008).

## 1 Introduction

In Namibia, widespread calcretes, together with (spatially) more restricted silcretes, are among the most auspicious features of the Cenozoic surface cover and are outcropping along deeply incised ephemeral or fossil drainage systems in terms of their ability to record past environmental change (Miller, 2008; Candy et al., 2004; Summerfield, 1983a; Van Der Wateren and Dunai, 2001; Ward, 1987). As well as being an important component in explaining the generally low denudation rates due to their protective function (Stokes et al., 2007; Nash and Smith, 1998), these silcretes and calcretes are also thought to indicate relatively long periods of landscape and climate stability during their formation (Goudie et al., 2015).

In general, calcretes are thought to form under semi-arid to arid conditions, with varying interpretations and associations with specific precipitation ranges (Goudie, 2020; Summerfield, 1983a; Alonso-Zarza, 2003). Various models have been proposed to explain the different types of calcrete (pedogenic, non-pedogenic, Goudie, 2020). In this study, we will mainly focus on the non-pedogenic, groundwater-related calcrete formation, based on the per ascensum hypothesis (Goudie, 1996; Goudie et al., 2015), which are formed mainly by evaporation from the capillary fringe or below the water table due to changing CO<sub>2</sub> level (Goudie et al., 2015). Most prominent calcrete formations are related to calcretes capping the Karpfenkliff Conglomerate of the Kuiseb Canyon in the central Namib and the Kamberg Calcrete Formation (Fig. 1, Ward, 1987). Secondary silcrete formation by pressure solution and reprecipitation was synchronous with calcrete formation in the Karpfenkliff conglomerates. It consists of microscale silcrete with discrete multiple layers of silcrete encrusting quartz clasts. The Karpfenkliff Conglomerate overlies the Tsondab Sandstone and was probably deposited in proto-Kuiseb and proto-Gaub valleys (Ward et al., 1983; Miller, 2008; Ward, 1987).

Calcretes in the central Namib are thought to be at least Early Pleistocene to Pliocene in age (Ward, 1987; Miller, 2008). Common dating techniques used to date calcretes are radiocarbon <sup>14</sup>C, U/Th disequilibrium, or solution U–Pb. The first two dating methods are limited to ~ 45 kyr or 500 kyr, respectively. Calcrete U–Pb laser ablation (LA) has recently been used to provide critical chronological information on the age–depth relationship of the calcretised sediments from the Kalahari Group (Houben et al., 2020). However, the dating of calcretes using the U–Pb system may be influenced or biased by detrital components from the source area of the leached carbonates. The variable growth rate makes it difficult to obtain individual ages from multiple generations of calcrete formation when using the bulk sampling approach for solution U–Pb dating, as it can be affected by the “nugget” effect (Branca et al., 2005). Although calcrete formation pre-dates the major canyon incision that can be dated using TCN exposure dating, calcrete formation post-dates sediment deposition and is not age equivalent to the host sediments. However, the time lag between sediment deposition and calcrete formation may be negligible for any expected age in the range of several millions of years. To avoid contamination by detrital components from the catchment and to date multiple stages of silcrete or calcrete formation, syndepositional (with calcrete formation) microscale silcretes produced by the secondary effect of calcrete formation, pressure solution and re-precipitation in the proximity (pressure shadow) might be a valuable target.

Evidence for climate change and major landscape change, as well as the reliability of dating of Pliocene and Pleistocene sediments in the Namib, is relatively poor and not well constrained, and in part it shows discrepancies between different dating techniques and interpretations (Miller, 2008; Van

Der Wateren and Dunai, 2001; Goudie and Viles, 2014). In Namibia, calcretes and silcretes commonly form prominent landscape features (i.e. cliffs) outcropping along deeply incised ephemeral or fossil drainage systems (Miller, 2008; Van Der Wateren and Dunai, 2001; Ward, 1987). The (relative) chronology of these fossil duricrusts is the backbone of the (late) Cenozoic chronostratigraphy of the Namib Desert (“Namib Group” of Miller, 2008) and past climate reconstructions (Miller, 2008, and references therein). A major weakness of this chronostratigraphy is its absolute chronology: essentially all early Quaternary to mid-Miocene continental deposits in the Namib Desert are “dated” with ostrich shells (Miller, 2008) or are age-correlated with deposits dated with such shells (Miller, 2008). In general, the ostrich shell biostratigraphy is linked to intracontinental correlations derived from fossil mammals (Pickford and Senut, 2000). The catch is that only the oldest shells are “dated” to 16–20 Ma (Aepyronithoid, Senut, 2000; Pickford et al., 1999, 1995), whereas the ensuing eight ostrich species are arbitrarily assigned to 2 to 3 Myr long periods (Senut, 2000) without any direct age control. The ostrich shell biostratigraphy provides a valuable relative chronology, but its use in its current form as an absolute chronology remains unverified for the time < 16 Ma. Consequently, the generally accepted Late Cenozoic chronostratigraphy of the Namib Desert (Miller, 2008) requires verification.

The use of terrestrial cosmogenic nuclide (TCN) exposure dating in the Namib Desert has grown in recent years, demonstrating that this method is a reliable way to measure landscape change (Van Der Wateren and Dunai, 2001; Vermeesch et al., 2010; Stone, 2013; Bierman and Caffee, 2001). According to Van Der Wateren and Dunai (2001), major changes in the Namib Desert, i.e. rejuvenation of the landscape by intermittent fluvial phases during the predominant arid to hyperarid climate, indicate major changes during the Pliocene and Pleistocene. However, there are doubts about the interpretation of the exposure ages in relation to the underlying deposited sediments (Miller, 2008). The dating of groundwater connected silcretes and calcretes beneath the surfaces sampled for TCN exposure dating allows us to verify the resulting TCN exposure ages. Furthermore, the combination of both dating techniques can be used to build a robust chronology of landscape change during the evolution and intensification of arid conditions in the Namib Desert.

Here we present the new application of U–Pb laser ablation to groundwater silcretes from the Namib Desert in combination with remeasured TCN exposure ages from the Carp Cliff and nearby equivalent sites. Laser ablation U–Pb dating of multiple microscale silcrete layers from the Karpfenkliff Conglomerate Formation indicates groundwater calcrete and silcrete formation during the Pliocene. Remeasured surface clasts from Van Der Wateren and Dunai (2001) confirm and substantiate the interpretation of a major landscape rejuvenation of the central Namib during the Pliocene–Pleistocene transition. The combination of the two dating techniques al-

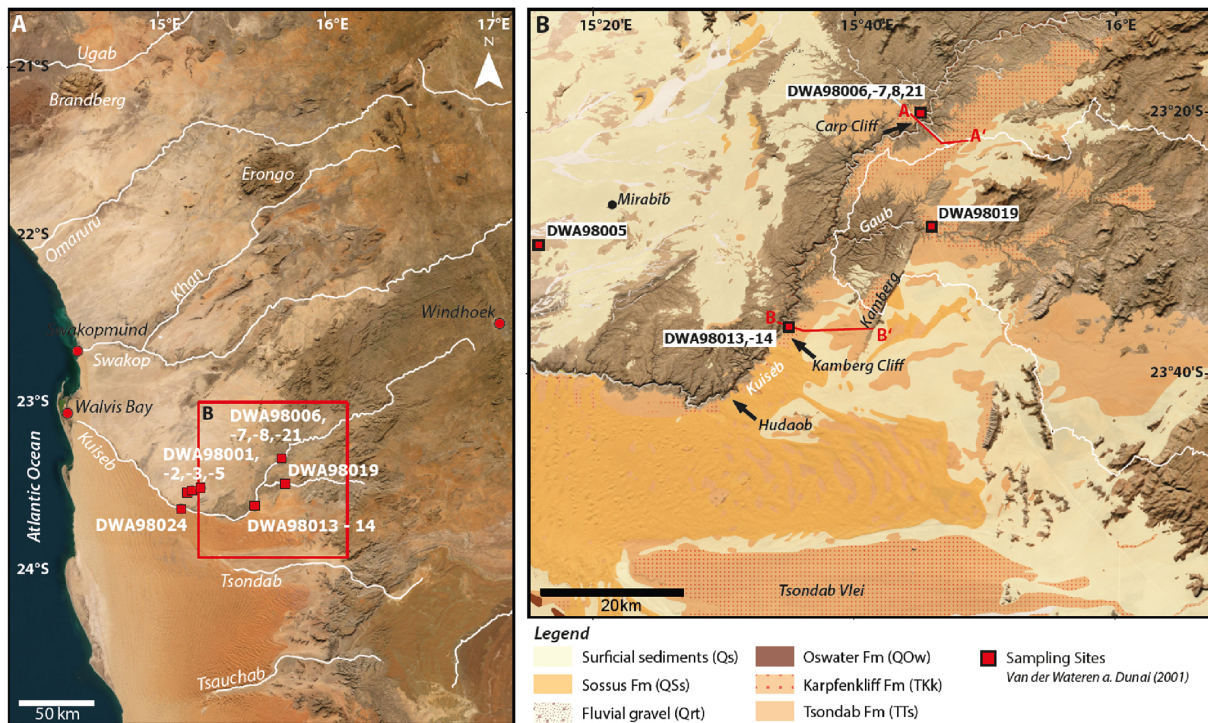


**Figure 1.** (a) Overview map of the central Namib Desert based on World Imagery (Earthstar Geographics (TerraColor NextGen) from ArcGIS Pro Version 3.1.0). Major drainage systems are shown in white. Red rectangle indicates the study area. Red squares indicate sampling sites of Van Der Wateren and Dunai (2001). Topographic profiles in Fig. 2 are marked as red lines. (b) The study area (Earthstar Geographics (TerraColor NextGen) imagery, ArcGIS Pro Version 3.1.0) including mapped geology by the Geological Survey of Namibia (Geological Survey of Namibia, 2016). Relevant geological formations are shown covering the Cenozoic sediment succession of the central Namib (Namib Group). Red squares indicate sampling sites from Van Der Wateren and Dunai (2001). The sub-catchment of the Gaub River is shown in white.

allows a robust chronological reconstruction of landscape evolution and the paleoclimate transition to increasingly arid conditions in the central Namib Desert.

## 2 Sampling site and samples

The central Namib Desert, between the Atlantic Ocean to the west and the Great Escarpment to the east, is a relatively flat landscape with numerous dispersed inselbergs and locally deeply incised canyons formed by ephemeral rivers such as the Kuseb or Swakop (Fig. 1). Our study focuses on the Kuseb River canyon in the central Namib. The ephemeral Kuseb River marks the prominent boundary between the stone desert in the north and the Namib Sand Sea to the south. The Kuseb River receives its water from precipitation in the Great Escarpment to the east, with mean annual rainfall of 200–450 mm yr<sup>-1</sup> (Ward, 1987; Jacobson et al., 1995). Annual floods of the Kuseb River clean its bed of all sand transported from the Namib Sand Sea to the south. They only reach the sea during exceptionally high floods (Van Der Wateren and Dunai, 2001). The Kuseb River forms a distinctive deep and partly narrow canyon, which is up to 250 m deep and only 1000 m wide at its deepest part (Figs. 1, 2). The

recent course of the Kuseb River is south-southwest to Hudaob, where it is thought to have been redirected northwest by the activity of the Namib Sand Sea (Miller, 2008). Prior to this deflection, the Proto-Kuseb River may have flowed westwards, as indicated by numerous outcrops within the inter-dune valleys of the Namib Sand Sea (Fig. 25.18 Vol. 3 in Miller, 2008; Ward, 1987; Lancaster, 1984).

### 2.1 Sediment succession in the Kuseb Canyon

The outcrop sequence along the Kuseb canyon in our study area comprises up to 100 m of sedimentary units (Fig. 2) resting on the Namib Unconformity Surface of Precambrian age (NUS, Ward, 1987; Miller, 2008), consisting of basal breccias from Precambrian basement and solidified aeolian sands assigned to the Tsondab Sandstone Formation overlain by calcretised coarse-grained conglomerates, called the Karpfenkliff Conglomerate Formation (Ward, 1987). Well-preserved terraces, resistant to weathering due to calcretisation, are exposed at the rim of the canyon (Fig. 3).

The Tsondab Sandstone Formation rests on the Namib Unconformity Surface (NUS, Ward, 1987; Miller, 2008) and is the oldest and first terrestrial Cenozoic deposit in the cen-

tral Namib (Ward, 1987; Miller, 2008), covering large areas of the central Namib (Figs. 1, 2). The Tsondab Sandstone Formation consists predominantly of cemented aeolianites (Miller, 2008; Ward, 1987) and is regarded as the precursor of the recent Namib Sand Sea (Ollier, 1977). The Tsondab Sandstone Formation is thought to have been deposited under predominantly arid conditions (Ward, 1987) between 20–16 and 5 Ma based on the biostratigraphy of *Struthious* eggshells (*Namornis oshanai*, *Struthio karingarabensis*, Ward and Corbett, 1990; Pickford et al., 1995; Senut, 2000).

## 2.2 Proto-Kuiseb Incision and aggradation of the Karpfenkliff Conglomerate Formation

The Karpfenkliff Conglomerate Formation (TKk, Ward, 1987) overlies the Tsondab Sandstone Formation and was deposited in a proto-Kuiseb and proto-Gaub River valley, a tributary of the Kuiseb River (Figs. 1, 2). Pre-depositional incision of the Kuiseb and Gaub rivers probably occurred during a wetter phase (Ward, 1987; Miller, 2008). The incision excavated a broad shallow valley and eroded the semi-consolidated Tsondab Sandstone without eroding the underlying Precambrian Damaran schists (Ward, 1987; Miller, 2008). The Karpfenkliff Conglomerate Formation consists of a medium- to fine-grained, sand-sized matrix of angular to subrounded clasts (Fig. 3, Ward, 1987; Miller, 2008). Clasts are rounded to well rounded with numerous percussion marks (Ward, 1987; Van Der Wateren and Dunai, 2001). The Karpfenkliff Conglomerate Formation thins to the west, indicating a depositional wedge (Miller, 2008). The thickest accumulations are found at the foothills of the Great Escarpment (~ 60 m, Miller, 2008), decreasing to ~ 40 m (Ward, 1987) in the upper Gaub Valley, 20–30 m at the Karpfenkliff and thinning to ~ 5 m at Gomkaeb (Ward, 1987; Miller, 2008). Deposition took place in a wide, shallow, braided river system (Ward, 1987; Miller, 2008), presumably during an intermittent pluvial phase despite prevailing arid conditions and synchronous with the deposition of the Tsondab aeolianites (Ward, 1987). Equivalent gravels in the Tsondab, Tsauchab and Swakop rivers are assigned to the Karpfenkliff Conglomerate Formation (Miller, 2008). The conglomerate is cemented by a massive groundwater calcrete that has caused significant volume expansion (Miller, 2008). The source area of the carbonate ions is thought to be the outcropping and eroding Precambrian Nama Group in the headwaters of the Kuiseb River and is therefore authigenic in origin. Calcretisation caused secondary precipitation of microscale silcrete by pressure solution and local re-precipitation.

The Karpfenkliff Conglomerate Formation is age-correlated with the occurrence of *Diamantornis corbetti* (fossil ostrich shell) in the Tsondab Aeolianites at Elim (Pickford and Senut, 2000; Miller, 2008), implying a younger age of *Diamantornis corbetti* than 14–15 Ma, equivalent to the age of the Arries Drift Formation (Miller, 2008). The youngest deposition age (prior to  $2.81 \pm 0.11$  Ma) was proposed by

Van Der Wateren and Dunai (2001) based on  $^{21}\text{Ne}$  exposure dating of abandoned surfaces of the Kuiseb River. The latter indicates the minimum depositional age for the last remnants of any fluvial transport and deposition of the Karpfenkliff Conglomerate Formation. Although this age is controversial according to Miller (2008, p. 25–27) based on the ostrich shell biostratigraphy, it clearly indicates the onset of incision by the recent Kuiseb River.

## 2.3 Calcrete within Karpfenkliff Formation and Tsondab Sandstone – Kamberg calcrete formation

The Kamberg Calcrete is described as a pedogenic calcrete up to 5 m in thickness (Miller, 2008; Ward, 1987; Yaalon and Ward, 1982). According to Miller (2008), it cements the upper Karpfenkliff Conglomerate Formation in places, as well as the Tsondab Sandstone, which covers a large area east of Homeb in the Kuiseb River (Miller, 2008; Ward, 1987; Yaalon and Ward, 1982). The Kamberg Calcrete, as well as equivalent calcretes in the study area, represent the surface predating the recent canyon incision of the Kuiseb and Gaub rivers. They are used as an important stratigraphic marker horizon in the Cenozoic “Namib Group” (Miller, 2008; Ward, 1987). Whether the Kamberg Calcrete is identical to the calcrete of the Karpfenkliff can be questioned (Fig. 2). The pedogenic Kamberg Calcrete may be transitional to the groundwater calcrete found at the Carp Cliff and therefore be syndepositional. If the Kamberg Calcrete at the key site at Kamberg correlates with the Kamberg Cliff and the Carp Cliff at Kuiseb canyon, this would imply that it is stratigraphically equivalent to or younger than the groundwater calcrete cementing the Karpfenkliff Conglomerate Formation (Fig. 2). A late Miocene age has been suggested for the evolution of the Kamberg Calcrete (Yaalon and Ward, 1982; Ward, 1987). The calcrete is thought to have been formed under semi-arid conditions during a relatively long period of landscape stability (Goudie et al., 2015; Ward, 1987), with seasonal precipitation of potentially 350–450 mm in the headwaters, decreasing drastically to the west (Ward, 1987).

A clear differentiation between the Kamberg Calcrete and any calcretes overlying and/or within the Karpfenkliff Conglomerate Formation is difficult. The Kamberg Calcrete is not specifically mapped in the published geological maps (Geological Survey of Namibia, 2016). For our study, we focused on near-surface clasts with silcrete at the Carp Cliff. The clear spatial and evolutionary differentiation, as well as the connection between the two, should be the focus of future research to use their occurrence as a marker horizon in the central Namib.

## 2.4 Kuiseb Incision – phase of landscape rejuvenation

The incision of the Kuiseb River (and other adjacent rivers such as the Swakop to the north) is thought to have begun

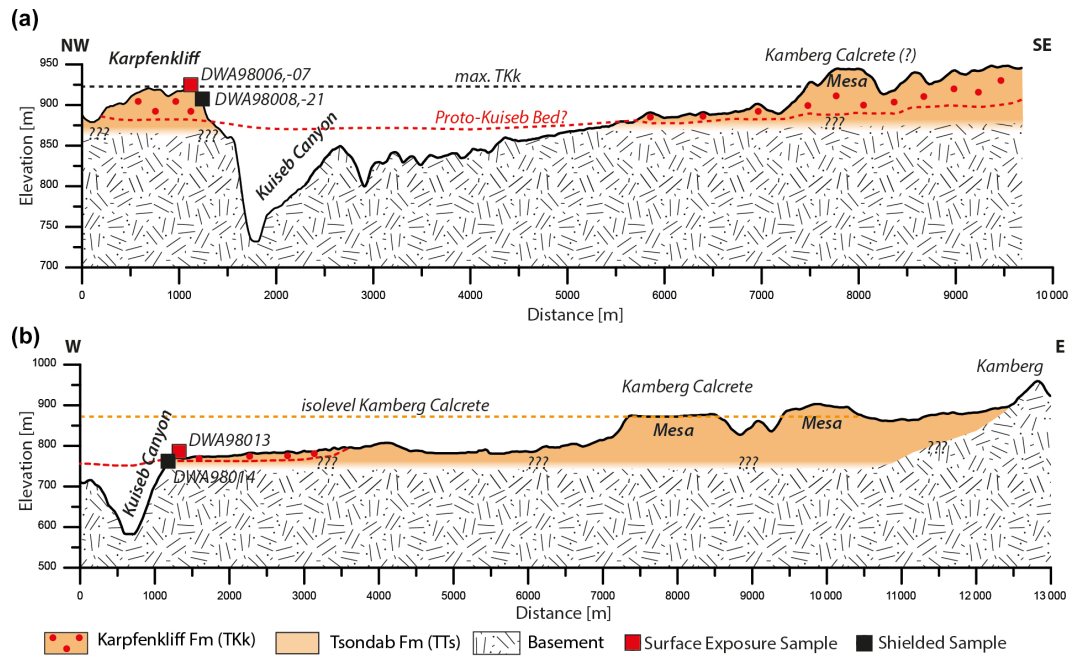


**Figure 2.** (a) Cross sections of the Carp Cliff and (b) Kamberg Cliff based on SRTM data (created using ArcGIS Pro 3.1.0). Spatial information on geological units was extrapolated from mapped geology (Geological Survey of Namibia, 2016). Samples were collected from the surface of the Carp Cliff (DWA98006,07) and from the subsurface at the canyon outcrop (DWA98008, -21). The identical sampling approach was used on the Kamberg Cliff by sampling exposed quartz clasts (DWA98013) and shielded clasts (DWA98014). The shielded quartz clasts were used to investigate and date secondary microscale silcrete layers attached to quartz clasts. Due to the unknown fluvial topography of the Proto-Kuseib, the profile is just an approximation. The occurrence of the Karpfenkliff Conglomerate Formation (TKk) is used from the geological map; however, its outcrop condition in profile A in the eastern sector remains speculative. The exact transition from the underlying Tsondab Sandstone (TTs) to the Karpfenkliff Conglomerate Formation is unclear and is approximated. The elevation of the Kamberg Calcrete from its key position is marked in (b) to illustrate the potential discrepancy between the two formations.

at the end of the Neogene, synchronous with other major river systems in South Africa (Ward, 1987; King, 1951; Partridge and maud, 1987; Korn and Martin, 1957). The recent incision was able to cut deeply into the Karpfenkliff Conglomerate Formation, the Tsondab Sandstone Formation and also the Precambrian Damaran schists (Miller, 2008; Van Der Wateren and Dunai, 2001; Ward, 1987), forming a V-shaped valley and the famous Kuseib canyon (Fig. 3). The transition from the aggradation of the Karpfenkliff Conglomerate Formation and the formation of calcretes, to the degradation and incision of the recent Kuseib, Gaub and Swakop rivers is thought to be related to either a tectonic- (King, 1955; Ward, 1987; Korn and Martin, 1957) or climatic control (Van Der Wateren and Dunai, 2001; Allen, 1989; Weissel and Seidl, 1998).

## 2.5 Detailed sampling sites and sampling

We consider the calcrete at our sampling sites (Carp Cliff and Kamberg Cliff, Figs. 1, 2, 3) to have been formed primarily by groundwater interaction due to its direct location near the present-day Kuseib canyon. We used sampled and dated (in situ  $^{21}\text{Ne}$ ) surface quartz clasts from Van Der Wateren and

Dunai (2001) of abandoned exposed surfaces and shielded clasts from several metres below the surface. Details of the sampling procedure and sampling sites are given in Van Der Wateren and Dunai (2001). For this study we concentrated on surface quartz clasts from the Carp Cliff (DWA98006, -07, -08, -21) and the Kamberg Cliff (DWA98013, -14) for remeasurement of cosmogenic  $^{21}\text{Ne}$  concentrations (Table 1). Eight quartz clasts from the Carp Cliff with visible silcrete cementation were prepared for U–Pb laser ablation (DWA98008, Table 1). The following descriptions are taken from Van Der Wateren and Dunai (2001) and partly adapted for additional samples.

## 2.6 Carp Cliff (Kuseib highest terrace)

DWA98006-07 (Site 6) is located on the horizontal upper surface of a mesa-shaped terrace remnant 500 m west of the 200 m deep Kuseib Canyon (Figs. 1, 2). The terrace has a surface area of  $\sim 5 \text{ km}^2$  and is surrounded by steep, locally vertical and overhanging cliffs, which to the east and south are nearly 50 m in height. The terrace surface consists of a desert pavement of mainly quartz pebbles overlying up to 15 cm of sandy silt. This is underlain by 10–25 m of calcretised pebble



**Figure 3.** Outcrop image compilation. (a) From Van Der Wateren and Dunai (2001) Kamberg Cliff showing  $\sim 15$  m of Karpfenkliff Conglomerates overlying  $\sim 15$  m of Tsondab Sandstones. (b) Carp Cliff (Field Campaign 2018; photo credit: Benedikt Ritter). (c) Close-up view of the calcrete-cemented Karpfenkliff Conglomerate Formation (photo credit: Benedikt Ritter). Rounded quartz clasts float in a matrix-supported fabric cemented by calcrete. Some clasts are fractured by volume expansion of the calcrete, resulting in pressure solution and formation of microscale silcrete. (d) Surface of the calcrete-cemented Carp Cliff (photo credit: Benedikt Ritter).

and boulder conglomerates of the Karpfenkliff Conglomerate Formation (Fig. 3). Van Der Wateren and Dunai (2001) collected 40 rounded (DWA98007) and (sub-)angular pebbles (DWA98006) with diameters between 2 and 6 cm. The site is located at the top of the mesa and is almost horizontal, meaning that post-depositional transport of the sampled pebbles by the Kuiseb River or local precipitation can be excluded.

DWA98008 and DWA980021 (sites 7 and 19) are located next to small gullies running from the northern side of the Carp Cliff mesa. At these sites, Van Der Wateren and Dunai (2001) collected shielded samples 5 m below the terrace surface. Van Der Wateren and Dunai (2001) sampled rounded pebbles from the ceilings of overhangs to ensure that the measured  $^{21}\text{Ne}$  concentrations were derived only during hillslope and fluvial transport to their present site and not from subsequent exposure at the sampling site.

### 2.7 Kamberg Cliff (Kuiseb highest terrace)

DWA98013 and DWA980014 are from a terrace on the Karpfenkliff Conglomerate Formation immediately adjacent to the nearly 250 m deep Kuiseb Canyon, 30 km downstream of Carp Cliff (Figs. 1, 2, 3). The terrace surface is very similar to that of Carp Cliff, with a desert pavement of pebbles and cobbles on a sandy silt overlying 25 m of calcretised

conglomerates. The Karpfenkliff Conglomerates rest on 30–50 m of the Tsondab Sandstone Formation, which forms the bulk of the cliff adjacent to the canyon. The DWA98013 sampling site is on the horizontal surface of the terrace, where we sampled angular pebbles. At DWA98014, rounded pebbles (DWA98014) were sampled from the ceiling of an overhang in the cliff face 6 m below.

### 3 Formation of calcretes and microscale silcretes

In general, two types of calcretes can be differentiated, pedogenic and groundwater calcretes (Alonso-Zarza and Wright, 2010), following the per descensum or the per ascensum evolutionary model (Goudie, 2020). They occur preferentially in arid to semi-arid climates (Alonso-Zarza, 2003; Candy and Black, 2009; Goudie, 2020). Specific climatic and environmental conditions are required for calcrete formation: (1) precipitation in the headwater or source area to promote carbonate dissolution and (2) intermittent or seasonal precipitation downstream to favour groundwater systems capable of (3) causing high evaporation and evapotranspiration for chemical precipitation of carbonate (Mann and Horwitz, 1979). Calcrete formation is dependent on the supply of carbonate ions leached from the drainage bedrock. In this study we focus on groundwater calcretes formed along the Kuiseb

**Table 1.** General sample information.

TCN exposure dating					
Sample ID	Locality	Type	Longitude (°)	Latitude (°)	Remark
DWA98006Etch2	Carp Cliff	Quartz clasts	−23.339	15.744	Amalgamated sample of 40 clasts
DWA98007Etch	Carp Cliff	Quartz clasts	−23.339	15.744	Amalgamated sample of 40 clasts
DWA98008Etch2	Carp Cliff	Quartz clasts	−23.331	15.746	Amalgamated sample of 40 clasts
DWA98021Etch	Carp Cliff	Quartz clasts	−23.332	15.745	Amalgamated sample of 40 clasts
DWA98013Etch2	Kamberg Cliff	Quartz clasts	−23.608	15.580	Amalgamated sample of 40 clasts
DWA98014Etch	Kamberg Cliff	Quartz clasts	−23.608	15.580	Amalgamated sample of 40 clasts
U–Pb LA-ICP-MS dating					
DWA98008- Silc3	Carp Cliff	Silcrete on clast	−23.331	15.746	Silcrete with distinct layering
DWA98008- Silc4	Carp Cliff	Silcrete on clast	−23.331	15.746	Silcrete with distinct layering
DWA98008- Silc7	Carp Cliff	Silcrete on clast	−23.331	15.746	Silcrete with distinct layering
DWA98008- Silc8	Carp Cliff	Silcrete on clast	−23.331	15.746	Silcrete with distinct layering

and Gaub rivers. Groundwater calcretes form at or above shallow groundwater tables and aquifers (Mann and Horwitz, 1979; Netterberg, 1969) and do not require subaerial exposure, although shallow contacts and stable surfaces favour the evolution of groundwater calcretes (Alonso-Zarza, 2003). They were originally called “valley calcretes” (Butt et al., 1977) because of their relationship with drainage. Groundwater calcretes are instead restricted to local drainage, although groundwater calcretes can have lateral extents of more than 100 km long and 10 km wide, depending on the drainage topography (Mann and Horwitz, 1979). Groundwater calcretes do not have characteristic features compared to pedogenic calcretes and are rather massive bodies (Alonso-Zarza, 2003). The permeability (coarse channel sediments) of the host rock favours their formation (Alonso-Zarza and Wright, 2010). Calcretes have been frequently used to obtain paleo-precipitation information, but the specific ranges are still under discussion. The upper limit may be between 600 and 1000 mm yr<sup>−1</sup> (Mack and James, 1994). The lower limit may be as low as 50 mm yr<sup>−1</sup> (Goudie, 1973; Retallack, 1994).

Silcretes can form as duricrust due to the accumulation of secondary silica within a soil or host rock (Milnes and Thiry, 1992; Summerfield, 1983a). Prominent examples include silcretes from Australia (Milnes et al., 1991; Taylor and Eggleton, 2017) or the Kalahari Desert (Summerfield, 1983b; Nash and Shaw, 1998). In this study, we focus on microscale silcretes, which are formed by pressure solution (Mcbride, 1989; Rutter, 1983; Sorby, 1863; Wilson, 2020) due to calcrete cementation and volume expansion within the host rock or sediment and therefore cannot be directly compared to the commonly used term “silcrete”. Additional silica may be enriched in the groundwater due to increased pH (favouring the precipitation of calcite and the solution of silica, Goudie, 1983; Nash and Shaw, 1998). Microscale silcrete formation is therefore thought to be linked to paleo-environmental and

climatic conditions favourable to calcrete formation. Calcretisation involves the precipitation of CaCO<sub>3</sub> within the pore spaces of the host rock or sediment, causing significant volume expansion. A secondary effect of this process is to increase the differential pressure within the host rock or sediment, causing clast shattering, relocation and pressure solution at intergranular contacts (Sorby, 1863; Rutter, 1983). Increased stress at grain boundaries and intergranular contacts leads to dissolution, e.g. silica mobilisation. Mobilised solutions migrate to regions of lower compressive stress, the “pressure shadow”, to reprecipitate. Theoretically, depending on the remaining pore space, multiple pressure solution and reprecipitation cycles can be archived in the host rock as multiple silcrete layers or shells attached to quartz clasts.

#### 4 Dating of calcretes and silcretes

Quantifying the timing and duration of calcrete formation is quite difficult. Clear stratigraphic relationships with the overlying and underlying sediments are not straightforward, as groundwater calcrete, for example, forms within sediments deposited close to the surface. Numerous studies propose only relative age controls and estimates of the formation time, such as the application of the ostrich shell biochronostratigraphy used for the Namib Group (Pickford and Senut, 2000; Senut, 2000; Miller, 2008). Many attempts have been made to date this type of deposit using radiocarbon <sup>14</sup>C (e.g. Geyh and Eitel, 1997), U/Th (Kelly et al., 2000; Candy et al., 2004; Candy and Black, 2009) or U–Pb dating (Rasbury and Cole, 2009; Houben et al., 2020).

Silcretes are enriched in U relative to calcretes and occur in most soils in arid and semi-arid environments. Uranium decays to Pb isotopes through a chain of intermediate daughter isotopes, and ages of samples from thousands to millions of years old can be estimated using parent–daughter pairs, such as <sup>238</sup>U–<sup>206</sup>Pb, <sup>235</sup>U–<sup>207</sup>Pb, <sup>234</sup>U–<sup>230</sup>Th

and  $^{238}\text{U}$ – $^{234}\text{U}$ . The use of a particular isotope pair depends on how old the sample is compared to the half-life of the selected radioactive isotope within the U decay chain (Neymark, 2011; Neymark et al., 2002, 2000). Considering that the samples are 2.85 Ma old or older (Van Der Wateren and Dunai, 2001), the U–Pb method using the parent–daughter pairs  $^{238}\text{U}$ – $^{206}\text{Pb}$  and  $^{235}\text{U}$ – $^{207}\text{Pb}$  was chosen to date the samples in this work.

Many studies attempting to date massive calcretes and silcretes are hampered by the dilution or averaging effect of bulk analysis and by bias from non-carbonate detrital minerals or secondary reprecipitated carbonate due to diagenesis. The “limestone dilution effect” (as a result of contamination with detrital carbonate components of the host rock, Alonso-Zarza, 2003) or the “averaging effect” (averaging of different phases of mineral precipitation, Candy and Black, 2009; Neymark et al., 2000) are minimised (or even avoided) by the higher spatial resolution of laser ablation compared to bulk analysis techniques. The possible effect of detrital components (e.g. zircon or clay minerals) on the U–Pb analyses is also neglected, as the signals from these inclusions can be filtered out of the time-resolved analyses.

The conventional method of calculating U–Pb isotope dates assumes that all intermediate daughter isotopes in the  $^{238}\text{U}$  and  $^{235}\text{U}$  decay chains were in secular equilibrium at the time of formation (Neymark, 2014). This is not necessarily true for calcretes and silcretes due to differences in the geochemical behaviour of parent and daughter elements. The silcretes dated in this study are sufficiently old (> ca. 2.85 Ma) to have achieved secular equilibrium (at present) and therefore for (almost) all of its initial excess of daughter isotopes to decay or for their initial depletion to replenish (i.e. their activity ratios to be equal to 1); thus, a direct measurement of these deviations is not feasible. Therefore, the values needed to correct for these disequilibria were estimated from previous works (see Sect. 5).

## 5 Methods

### 5.1 Raman spectroscopy

We use Raman spectroscopy to obtain high-resolution images of silcretes and to better characterise the mineralogical composition. Raman spectra were collected with up to 1300 wavenumber ( $\text{cm}^{-1}$ ) using a WITec alpha 300R confocal Micro-Raman microscope at the Goethe University Frankfurt (GUF). The objective used was 50x, an excitation laser of 532 nm (using 10 mW laser power before the objective) and spectra integration time of 0.2 s, with five accumulations in total. Maps ( $400 \times 400 \mu\text{m}^2$ ) were performed applying a step size of  $1.3 \mu\text{m}$  with a holographic grating of  $600 \text{ grooves mm}^{-1}$ . The instrument was calibrated using an Ar–Hg spectral lamp and was checked regarding its performance before the measurements with respect to the  $1300 \text{ cm}^{-1}$  line of silicon. The spectrum of each sample layer

was confirmed at several locations on the same layer. Raman spectra of reference compounds are found in the Ruff database (<https://ruff.info/>, last access: 26 April 2023).

### 5.2 Dating of silcretes – U–Pb laser ablation inductively coupled plasma mass spectrometry (ICP-MS)

Eight quartz clasts were cut in half to expose their silcrete coatings, mounted in epoxy mounts and polished at the Department of Geosciences at the University of Cologne (UoC). U–Pb analyses were performed at the Goethe University Frankfurt (GUF) using a RESolution 193 nm ArF excimer laser (COMpex Pro 102), equipped with a two-volume ablation cell (Laurin Technic S155). The laser was coupled to a Thermo Scientific Element Xr sector field ICP-MS. The surfaces were cleaned with eight pre-ablation laser pulses. Ablation was carried out in a He ( $0.3 \text{ L min}^{-1}$ ), Ar ( $1.01 \text{ L min}^{-1}$ ) and N ( $0.012 \text{ L min}^{-1}$ ) atmosphere, with a high energy density (ca.  $5 \text{ J cm}^{-2}$ ), a frequency of 15 Hz and round  $50 \mu\text{m}$  diameter spots (Table S1 in the Supplement).

Artificial silicate glasses NIST SRTM 612 and 614 were used as reference materials (RM). Plots and dates are calculated using the in-house spreadsheet program (Gerdes and Zeh, 2009, 2006), together with Isoplot (Ludwig, 2012). Ages are reported with and without systematic components (i.e.  $\text{date} \pm 2 / 2 s_{\text{sys}}$ ). Uncertainties include internal standard error (SE), background, counting statistics, excess scatter of the primary reference material (NIST SRTM 612) and excess variance (calculated from NIST SRTM 614). Systematic uncertainties also propagate systematic errors, which are the long-term excess variance (1.5 %, 2 s), decay constant uncertainties (Horstwood et al., 2016) and the uncertainty derived from the initial activity ratio uncertainty. Dates are calculated as Tera–Wasserburg lower intercepts (Tera and Wasserburg, 1972). Linear regressions are anchored to a common lead  $^{207}\text{Pb} / ^{206}\text{Pb}$  ratio of 0.837. This is the y intercept of sample “DWA98008-Silc4 Black Crack”, which is where this ratio is better constrained. This value is in good agreement with modelled crustal values at the time of formation (0.836, Stacey and Kramers, 1975).

The samples dated are sufficiently old to have reached secular equilibrium, and hence activity ratios cannot be measured (with the present techniques and assuming a closed system behaviour). Consequently, the following initial activity ratios used are assumed. The silcretes dated in this study have virtually no Th (average of  $\sim 89 \text{ ng g}^{-1}$ ), and therefore we consider  $[^{230}\text{Th} / ^{238}\text{U}]_i = 0$  (initial  $^{230}\text{Th} / ^{238}\text{U}$  activity ratio). Considering previous studies on calcretes and silcretes formed in semi-arid and arid environments (Oster et al., 2017; Maher et al., 2007; Neymark, 2011), the ground and surface waters from which these rocks are formed often have  $[^{234}\text{U} / ^{238}\text{U}]_i$  values greater than 1. Therefore, the data in this study are calculated with  $[^{234}\text{U} / ^{238}\text{U}]_i = 1.75 \pm 0.32$  ( $2 s_{\text{abs}}$ ), which is a weighted average of the  $[^{234}\text{U} / ^{238}\text{U}]_i$  of the above-mentioned studies. The uncertainty in this ac-

tivity ratio is added to the final systematic uncertainties by quadratic propagation (Scardia et al., 2019; Table S2b).

### 5.3 Cosmogenic $^{21}\text{Ne}$ exposure dating

We used prepared samples from Van Der Wateren and Dunai (2001) for in situ  $^{21}\text{Ne}$  exposure dating using the new noble gas mass spectrometer at the University of Cologne (Helix MC Plus from Thermo Fisher Scientific; for further information, see Ritter et al., 2021). The  $^{21}\text{Ne}$  analyses of Van Der Wateren and Dunai (2001) were performed without an international standard (CREU). For neon analysis we prepared amalgamated samples from each site containing between 35 and 40 quartz clasts (100 mg per sample) using the already prepared 63–125  $\mu\text{m}$  fraction. By also analysing shielded pebbles, a pre-exposure correction (accumulated  $^{21}\text{Ne}$  concentration during transport) can be applied to analysed surface samples (Repka et al., 1997). The presumably non-atmospheric  $^{21}\text{Ne}$  concentration found in these samples can be subtracted from the concentration in their exposed counterparts. The latter also corrects for any potential nucleogenic  $^{21}\text{Ne}$  that may be present in the samples. Samples were measured on the noble gas mass spectrometer at the University of Cologne using the analytical methods outlined in Ritter et al. (2021). CREU quartz standards were measured in Cologne for interlaboratory comparability and quality control (Vermeesch et al., 2015). The spallogenic origin of the measured  $^{21}\text{Ne}$  excess was verified using the triple isotope plot. The  $^{21}\text{Ne}$  exposure ages were calculated using the “nuclide-dependent scaling” after Lifton et al. (2014), calculated with “the online exposure age calculator formerly known as the CRONUS-Earth online exposure age calculator” (Version 3, [http://hess.ess.washington.edu/math/v3/v3\\_age\\_in.html](http://hess.ess.washington.edu/math/v3/v3_age_in.html), last access: 10 September 2023; Balco et al., 2008).

## 6 Results

### 6.1 Silcrete imaging

Digital microscope images show vein contact parallel layering with different crystal orientations (Figs. 4a and S1). The Raman spectra peaks at 129, 209 and 467  $\text{cm}^{-1}$  are indicative of quartz, which dominate the silcrete samples. Raman spectroscopy of DWA98008-Silc8 also indicate the presence of one major calcite band (dark colour in Fig. 5b, Raman spectra peaks at 156, 283, 466, 714 and 1088  $\text{cm}^{-1}$ ). The calcite crack filling might be indicative for shattering of previous silcrete and crack filling by repeated and/or ongoing calcrete formation within the Karpfenkliff Conglomerate.

### 6.2 U–Pb laser ablation results – silcretes

Four out of the eight silcrete samples yielded meaningful dates (DWA98008 – Silc3, Silc4, Silc7, Silc8), out of which 12 dates could be calculated from various silcrete layers

(Table S2, Fig. S1). The dates range from  $2.96 \pm 0.14$  to  $6.72 \pm 0.16$  Ma, with maximum relative abundance peaks at around 3.4 Ma and about 5.5 Ma (see Fig. 6 and Table 2). All dates are calculated from multiple spot analyses, ranging from 9 to 28 spots per date. The majority of the analyses have U concentrations between  $\sim 30$  and  $70 \mu\text{g g}^{-1}$ , with an average of  $42 \mu\text{g g}^{-1}$ , and very low Th concentrations, up to  $200 \text{ ng g}^{-1}$ , with an average of  $89 \text{ ng g}^{-1}$ .

### 6.3 TCN exposure age results

The  $^{21}\text{Ne}$  samples measured at the Noble Gas Laboratory in Cologne (Ritter et al., 2021) yield concentrations of  $1.52\text{--}1.95 \times 10^7$  atoms per gram for shielded samples (DWA98008, 014, 021) and  $6.30\text{--}9.60 \times 10^7$  atoms per gram for surface samples (DWA98006, 007, 013). All samples are within  $2\sigma$  of the spallation line (Fig. 5). Compared to the  $^{21}\text{Ne}$  concentrations of Van Der Wateren and Dunai (2001), the etched samples measured in Cologne reveal lower concentrations of up to 13 % difference when comparing direct concentrations (average of five measured samples); however, within  $\pm 1\sigma$  it reduces to  $\sim 1.6$  %, agreeing within  $\pm 2\sigma$  on average. We have excluded sample DWA98008, as it presumably contains a high abundance of non-cosmogenic Ne, as deduced from the significant concentration differences between the sample measured by Van Der Wateren and Dunai (2001) and the etched counterpart measured in Cologne (Table S1). Similar results and interpretations for sample DWA98008 were reported by Van Der Wateren and Dunai (2001).

Using the mean difference of  $\sim 13$  % between VU Amsterdam and Cologne Ne concentrations (Table S1), the data from Van Der Wateren and Dunai (2001) can be corrected for lab-specific differences. The corrected exposure ages are given in Table 3.

Calculated exposure ages derived from Cronus Earth (Balco et al., 2008) are summarised in Table 3. For the Kuiseb terrace,  $^{21}\text{Ne}$  concentrations in shielded, pre-exposed samples (DWA98008, DWA98021) give a mean apparent age of  $0.65 \pm 0.04$  Ma (external uncertainty  $\pm 1\sigma$ ). The latter indicates that the non-cosmogenic component of DWA98008 has been removed by etching, indicating the identical apparent exposure age as DWA98021. Correction of the  $^{21}\text{Ne}$  concentration of exposed rounded pebbles (DWA98007) from the top of the Carp Cliff terrace yields an exposure age of  $3.2 \pm 0.2$  Ma ( $\pm 1\sigma$  external uncertainty), being slightly older than calculated by Van Der Wateren and Dunai (2001); however, they are identical within the uncertainty. Exposed angular clasts (DWA98006) show a younger exposure age of  $2.85 \pm 0.19$  Ma ( $\pm 1\sigma$  external uncertainty). The latter is slightly older than in Van Der Wateren and Dunai (2001), which is identical within their uncertainty. A similar exposure age of  $2.75 \pm 0.18$  Ma ( $\pm 1\sigma$  external uncertainty) was derived from angular clasts from the Kamberg Cliff (DWA98013). Angular clasts are assumed to be derived

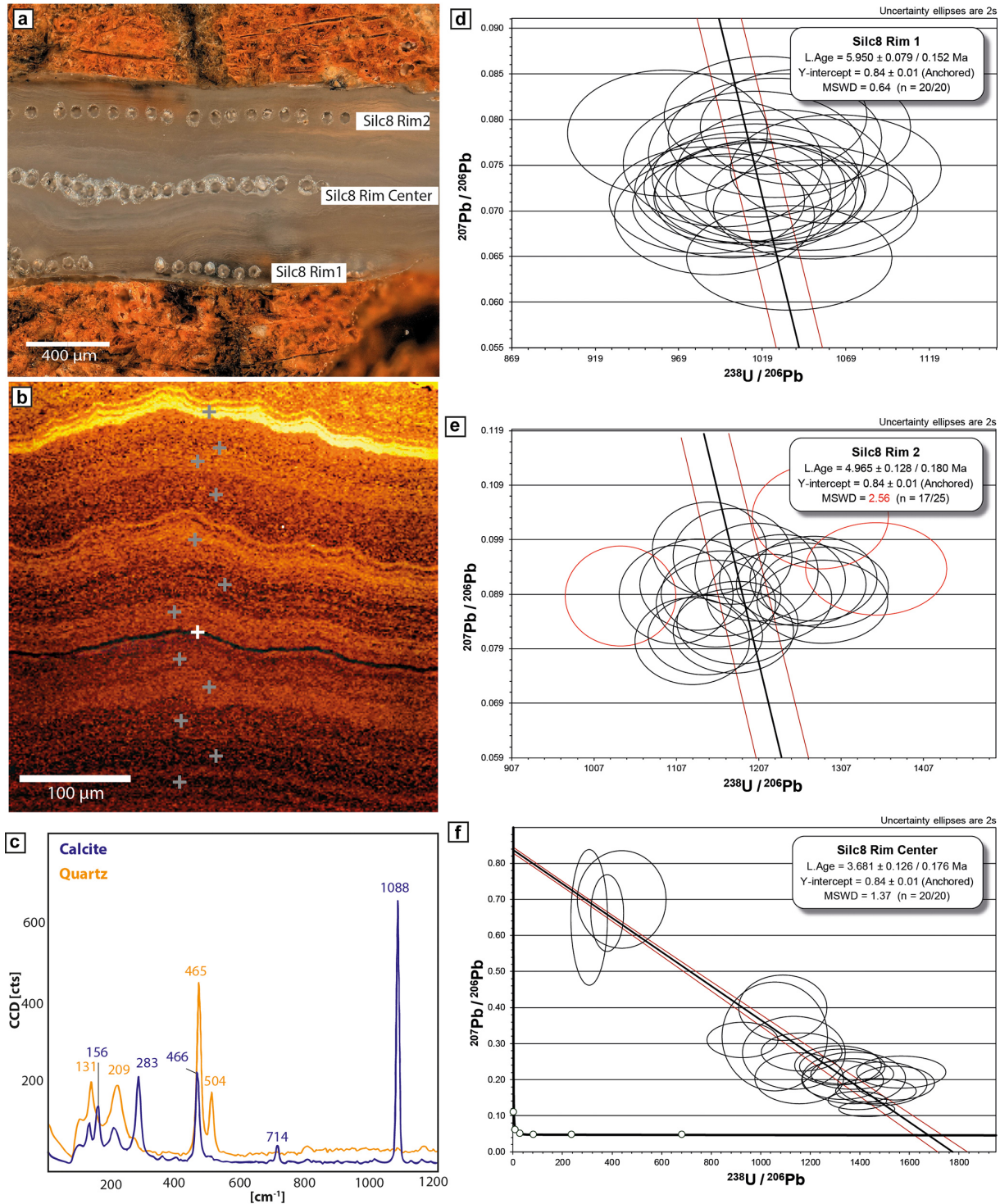


**Figure 4.** (a) Microscope image of sample DWA98008-Silc8 after LA-ICP-MS analysis. Laser spots are visible, and respective U–Pb Tera–Wasserburg plots are shown in (d–f). (b) Raman image of Silc8, area not visible on microscope image. Grey crosses indicate measured quartz spectra. White cross marked the occurrence of calcite, which can be traced as a black line. Raman imaging shows multiple layering of silcrete filling the crack of the shattered quartz clast. Colour variations are indicative of differences in crystal orientations (c) Respective Raman spectra for the quartz and calcite identification. (d–f) Tera–Wasserburg plots of Silc8 and respective U–Pb ages (red ellipses are considered outliers).

**Table 2.** (1) Concordia curve lower intercept dates from a Tera–Wasserburg diagram (Tera and Wasserburg, 1972). (2) The 2 s absolute uncertainties, considering within-run precision (SE of the mean of ratios), excess of scatter, background, counting statistics and excess of variance (calculated from the validating RM, SRTM NIST 614 of 2.6 %, 1 s, on  $^{238}\text{U} / ^{206}\text{Pb}$  and 0 %, 1 s, on  $^{207}\text{Pb} / ^{206}\text{Pb}$  ratios). (3) Previous uncertainties (2) expanded with systematic uncertainties (0.8 %, 2 s, long term reproducibility and decay constant uncertainties); see Horstwood et al. (2016). (4) The  $^{207}\text{Pb} / ^{206}\text{Pb}$  ratio of the upper intercept. (5) The 2 s absolute uncertainty of the upper intercept. (6) If the linear regression on the Tera–Wasserburg was anchored or not. (7) Mean squared weighted deviation. (8) Number of analyses considered. (9) Total number of analyses. (10) Dates calculated (following Wendt and Carl, 1985) taking into account an initial  $^{234}\text{U} / ^{238}\text{U}$  activity ratio of 1.75 and initial  $^{230}\text{Th} / ^{238}\text{U}$  activity ratios of 0. (11) Uncertainties (2) recalculated to the new dates (10). (12) Uncertainties (3) recalculated to the new dates (10) and adding  $^{234}\text{U} / ^{238}\text{U}$  activity ratio uncertainty (0.32, 2  $s_{\text{abs}}$ ).

Sample name	Date (Ma) (1)	2 $s_{\text{abs}}$ (2)	2 $s_{\text{sys}}$ (3)	y intercept (4)	2 s (5)	Anchored (6)	MSWD (7)	n (used) (8)	n (total) (9)	Date (Ma) (10)	2 $s_{\text{abs}}$ (11)	2 $s_{\text{sys}}$ (12)
Silc3 Rim 1	5.756	0.124	0.132	0.837	0.008	True	0.45	9	9	5.590	0.120	0.176
Silc3 Rim 2	5.246	0.107	0.115	0.837	0.008	True	0.41	9	9	5.080	0.103	0.164
Silc3 Rim 3	5.488	0.068	0.081	0.837	0.008	True	1.35	24	28	5.322	0.066	0.143
Silc3 Rim Outer	3.734	0.064	0.071	0.838	0.011	True	1.63	28	28	3.569	0.061	0.138
Silc4 Black Crack	5.927	0.244	0.248	0.8374	0.0066	False	1.50	21	25	5.761	0.237	0.270
Silc4 Rim	3.498	0.061	0.067	0.837	0.008	True	1.24	16	17	3.332	0.058	0.136
Silc4 Rim Outer	3.456	0.061	0.067	0.837	0.008	True	1.30	15	17	3.290	0.058	0.136
Silc4 Rim Inner	3.129	0.068	0.072	0.837	0.008	True	1.63	9	9	2.964	0.064	0.138
Silc7	6.881	0.091	0.106	0.8528	0.0028	False	0.94	27	29	6.715	0.089	0.159
Silc8 Rim Out 1	6.116	0.081	0.095	0.837	0.008	True	0.64	20	20	5.950	0.079	0.152
Silc8 Rim Out 2	5.131	0.132	0.139	0.837	0.014	True	2.56	17	25	4.965	0.128	0.180
Silc8 Rim Center	3.847	0.131	0.135	0.837	0.008	True	1.37	20	20	3.681	0.126	0.176

**Table 3.** TCN exposure ages.

	LSDn exposure age		
	Age (Ma)	Int. Unc. (Ma)	Ext. Unc. (Ma)
DWA98006Etch2	2.85	0.07	0.19
DWA98007Etch	3.85	0.07	0.25
Corr. DWA98007Etch2	3.20	0.05	0.20
DWA98008Etch2	0.66	0.02	0.05
DWA98021Etch	0.65	0.02	0.04
DWA98013Etch2	2.75	0.05	0.18
DWA98014Etch	0.90	0.02	0.06
DWA98001VU	5.35	0.23	0.41
DWA98002VU	3.98	0.32	0.40
DWA98003VU	1.08	0.13	0.15
DWA98005VU	0.58	0.06	0.07
DWA98019VU	0.49	0.05	0.06
DWA98024VU	1.27	0.12	0.14

from local sources without significant pre-exposure from long transport times. Our results indicate that terrace abandonment and exposure to cosmic rays started at  $\sim 2.8$  Ma (Fig. 6).

## 7 Interpretation and discussion

Our U–Pb ages are stratigraphically in the correct order, with the oldest U–Pb ages at the contact between quartz clast and filled rock fracture and the youngest age in the centre of the filled fracture (Table 2, Fig. 4). Recurrent U–Pb ages underpin and mark the main phase of silcrete, i.e. calcrete formation. Groundwater calcrete formation, i.e. microscale silcrete formation, within the sediments of the proto-Kuiseb canyon

(Karpfenkliff Conglomerate) took place between the Late Miocene ( $\sim 7$  Ma) and the Late Pliocene ( $\sim 3$  Ma, Fig. 6). The U–Pb silcrete ages suggest either persistent or alternating periods of wetter climate for groundwater calcrete formation.

Based on the causal relationship between silcrete and calcrete formation, our U–Pb silcrete ages indicate that environmental and climatic conditions during the Pliocene were sufficient to allow for carbonate leaching, transport and calcrete formation within the coarse-grained Karpfenkliff Conglomerate. However, whether the sampled groundwater calcrete is identical or synchronous with the prominent Kamberg Calcrete can be questioned, but we can narrow down the timing of major groundwater calcrete formation, previously assigned to the Late Miocene (Goudie et al., 2015; Ward, 1987) or Plio-Pleistocene (Pickford and Senut, 2000). Calcrete formation ceased during the Late Pliocene–Early Pleistocene by incision and groundwater lowering (Fig. 6).

Remeasured TCN  $^{21}\text{Ne}$  surface exposure ages from amalgamated quartz clasts agree with the derived U–Pb silcrete chronology and are younger than the youngest U–Pb silcrete age obtained (Fig. 6), i.e. in stratigraphically correct order. The surface exposure ages mark the abandonment of the fluvial terraces and the onset of the Kuiseb River incision at  $\sim 2.8$  Ma. The latter caused a groundwater lowering of the water table and the cessation of calcrete formation within the Carp Cliff Conglomerate Formation. Remeasurements of the quartz clasts from the Oswater terrace downstream of the Carp Cliff and Kamberg Cliff sampling sites confirm the exposure ages previously obtained by Van Der Wateren and Dunai (2001). The exposure ages of the Karpfenkliff and Os-

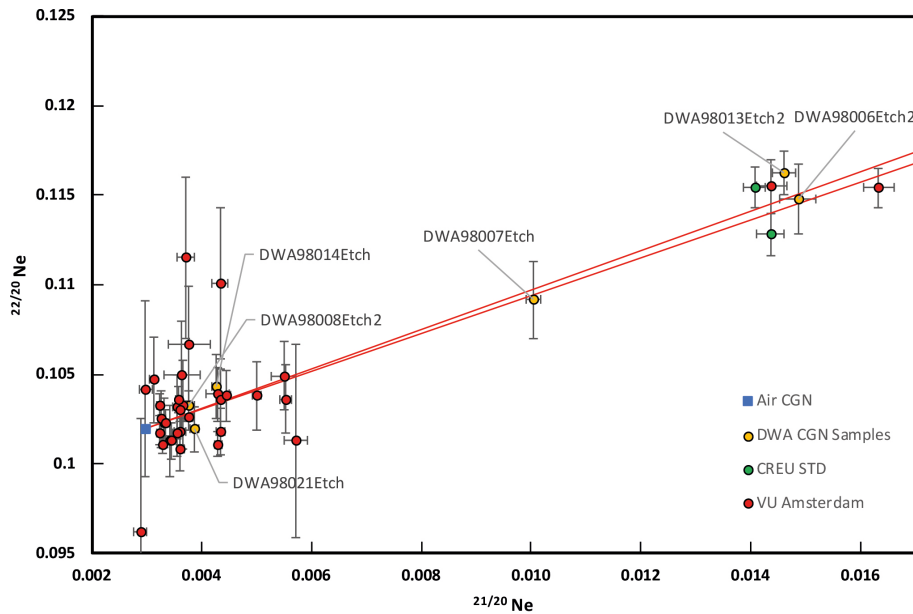


**Figure 5.** Triple isotope diagram indicating single heat step extraction of the Cologne laboratory (orange circles) compared to the multiple heat-step extraction (red circles) of Van Der Wateren and Dunai (2001). Uncertainties are  $1\sigma$ . The stippled red line indicates the Cologne laboratory spallation line (Ritter et al., 2021). Green circles indicate CREU1 measured during the analysis in Cologne.

water terrace constrain the period of major canyon incision to  $\sim 2.8$ – $1.3$  Ma (Fig. 6).

With the aid of absolute U–Pb silcrete and surface exposure dating, it is now possible to redefine depositional ages or depositional periods for sediments in the central Namib Desert, some of which are widely used as marker horizons. Our U–Pb silcrete ages constrain the timing of sediment deposition within the Kuiseb Canyon (Karpfenkliff Conglomerate Formation) to be older than  $\sim 7$  Ma, as silcrete formation within the conglomerates postdates deposition thereof (Fig. 6). The incision age of the Proto-Kuiseb and the subsequent deposition by the Karpfenkliff Conglomerate as proposed by Miller et al. (2021) of  $\sim 5$  Ma does not agree with our absolute U–Pb ages. If the relative biostratigraphic dating of Pickford and Senut (2000) is valid, the proto-Kuiseb canyon was filled by the Karpfenkliff Conglomerate Formation over a time period of up to 6–7 Ma (*Diamantornis corbetti* at Elim  $\sim 14$ – $15$  Ma; see Pickford and Senut, 2000). Verification and absolute direct dating of the Karpfenkliff Formation is still lacking and is a target for future studies. Our fluvial chronology substantially supports the chronological data obtained by Van Der Wateren and Dunai (2001).

### 7.1 Pliocene calcrete formation – steady-state climate

Our U–Pb ages indicate a relatively calm or transitional phase between aggradation and backfilling of the Proto-Kuiseb (and presumably other drainage systems such as the Swakop) and the renewed incision by the recent Kuiseb River throughout the Pliocene. U–Pb ages of microscale silcrete

from the same stratigraphic horizon indicate a long-term stable groundwater level, i.e. no significant aggradation or degradation.

As the formation of groundwater calcrete is generally restricted to specific environmental conditions, the existence and chronology of its formation in the central Namib Desert now allows us to relate these environmental conditions to specific episodes in the past and thus to obtain a better and partly more quantitative paleoclimate and environmental reconstruction of the Pliocene in the central Namib Desert. We therefore interpret our U–Pb silcrete chronology as marking the transition of the mean annual precipitation (MAP) from the upper potential limit of approximately  $\sim 600$  mm yr $^{-1}$  or the lower potential limit of 50 mm yr $^{-1}$  in the Kuiseb catchment during the Late Miocene. Whether there was a climate change from, or a return to, wetter conditions during the Pliocene cannot be determined from our U–Pb chronology. Calcrete formation ceased with the incision of the Kuiseb River and a significant lowering of the groundwater table.

Age information from the Kalahari Basin by Houben et al. (2020) indicated a shift towards more arid conditions since  $\sim 12$  Ma, which intensified at  $\sim 4$  Ma (Houben et al., 2020; Miller et al., 2010). Marine records off Namibia (Fig. 7, ODP 1081, Hoetzel et al., 2017) suggest a shift to more arid conditions over the course of the mid-Miocene to Late Miocene, controlled by a gradual increase in the upwelling activity of the Benguela Current, initiated by a strengthening of the meridional gradient. This shift is supported by pollen data (Hoetzel et al., 2015; Dupont et al., 2013), indicating the expansion of savanna grasslands (C<sub>4</sub>

expansion) in Namibia since  $\sim 8$  Ma, with a subsequent shift during the Pliocene to more shrubland and desert vegetation (Hoetzel et al., 2015). Compound-specific hydrogen isotopes (ODP 1085, Dupont et al., 2013) indicate a change in the precipitation source from the Atlantic to the Indian Ocean since  $\sim 8$  Ma (Dupont et al., 2013). Therefore, our U–Pb chronology of calcrete formation ( $\sim 7$ – $3$  Ma) tracks the shift to more arid conditions with a corresponding reduction in the MAP to allow calcrete formation. Nevertheless, this transition and aridification of the Namib was slow, and regional SST records (ODP 1082, Etourneau et al., 2009; ODP 1081, Rosell-Mel  et al., 2014, Fig. 7), as well as global paleoclimate records (benthic  $\delta^{18}\text{O}$ , Westerhold et al., 2020, Fig. 7), indicate a relatively stable climatic period. Rosell-Mel  et al. (2014) proposed, based on their marine SST record off Namibia (ODP 1082), that the persistently warm Pliocene, with conditions analogous to a persistent Benguela “El Ni o”, ended at the transition to the Pleistocene (Fig. 6).

## 7.2 Pliocene–Pleistocene transition

During the transition from the late Pliocene to the early Pleistocene, the central Namib Desert underwent large-scale landscape rejuvenation with drainage reorganisation and incision. This is the same period, in which Miller et al. (2010) reconstructed the major desiccation of the Etosha paleolake (Fig. 6). Based on U–Pb calcrete ages from the Kalahari Basin, Houben et al. (2020) proposed an intensification of arid conditions since  $\sim 3.8$  Ma, older than our onset of more arid conditions in the central Namib at around 3 Ma. Higher offshore sedimentation rates off Namibia may be associated with increased input of terrestrial material (Dupont et al., 2005) due to incision of E–W-flowing drainages into the Atlantic. The propagation of the Horingbaai fan delta (between Omaruru and the Ugab River) occurred approximately at the same time (2.7–2.4 Ma) according to Stollhofen et al. (2014), supporting the idea of large-scale landscape rejuvenation and incision of multiple E–W-flowing drainages in the Namib Desert.

The underlying mechanism is still questionable, as several forcing factors could be responsible for the incision of major E–W-flowing river systems: climate change and variability, sea level change, and/or tectonic uplift. The latter was previously suggested by Ward (1987) and attributed to a late Neogene epeirogenic uplift. Stollhofen et al. (2014) also suggest that uplift could be one of the causes and/or at least a contributor to other factors, such as climate.

Data from the marine realm off Namibia suggest a further step towards more extreme arid conditions during the Pliocene–Pleistocene transition (Fig. 6). Local SST records (ODP 1082, Etourneau et al., 2009; ODP 1081, Rosell-Mel  et al., 2014, Fig. 7) indicate the onset of decreasing SSTs at  $\sim 2.7$ – $2.5$  Ma and the significant shift towards increased upwelling activity of colder water masses in the Benguela Current since  $\sim 2.2$  Ma (Dupont et al., 2005; Marlow et al.,

2000; Etourneau et al., 2009). The significant decrease in SSTs correlates with the further intensification of Northern Hemisphere glaciation since  $\sim 2.7$  Ma (Ruggieri et al., 2009). The pollen record (ODP 1082) of Dupont (2006) shows that arid to semi-arid biomes were rather limited prior to  $\sim 2.7$  Ma and that their concentration increases with higher variability since then, reflecting the intensification of arid conditions in the central Namib Desert (Dupont, 2006).

Vegetation change may be a major cause of the exposure of landscapes to accelerated erosion. Major river incision in the central Namib Desert thus occurred during a period of climate change and greater climate variability compared to the more persistently stable Pliocene (Rosell-Mel  et al., 2014), with the intensification of arid conditions in southern Africa being synchronous with major global changes. We therefore propose that the major river incision of the Kuiseb River at the Pliocene–Pleistocene transition was caused by a shift to more arid conditions with decreasing precipitation, resulting in reduced river discharge, river steepening and incision (e.g. Whipple and Tucker, 1999; Bonnet and Crave, 2003; Molnar, 2001; Cooper et al., 2016). Catchment and river systems such as the Kuiseb (and/or river systems such as the Swakop), which had reached a steady state during the more stable Pliocene, had to adapt to the new boundary conditions, which is in line with the global increase in erosion rates at the Pliocene–Pleistocene transition (Herman et al., 2013; Herman and Champagnac, 2016). A major vegetation shift towards more arid biomes and sparser vegetation cover increased the susceptibility of landscapes to erosion. The global sea level drop at the Pliocene–Pleistocene transition may have had an additional impact on drainage base levels.

The incision of the recent Kuiseb River can be constrained to a period between the derived terrace ages of  $\sim 2.8$  and  $\sim 1.3$  Ma (minimum age of the Oswater bedrock river terrace). The actual period of incision may be even shorter, given the cessation of fluvial sediment deposition offshore at  $\sim 2$  Ma (Dupont et al., 2005). Deposition of the Oswater Formation indicates a phase of aggradation sometime after  $\sim 1.3$  Ma, followed by an incision into the recent bed of the Kuiseb River.

## 8 Conclusions

Our study demonstrates that microscale silcrete from the central Namib Desert can be dated using U–Pb LA-ICP-MS and that layered silcrete incrustations can be used as paleoclimate archives. LA-ICP-MS U–Pb dating of silcrete has advantages over bulk carbonate analysis because it is less affected by potential interferences and contamination. The combined dating approach with additional  $^{21}\text{Ne}$  exposure age dating allows us to reconstruct major paleoclimate and landscape changes since the Late Miocene for the central Namib Desert. We can corroborate previously obtained chronological data from Van Der Wateren and Dunai (2001) and place absolute

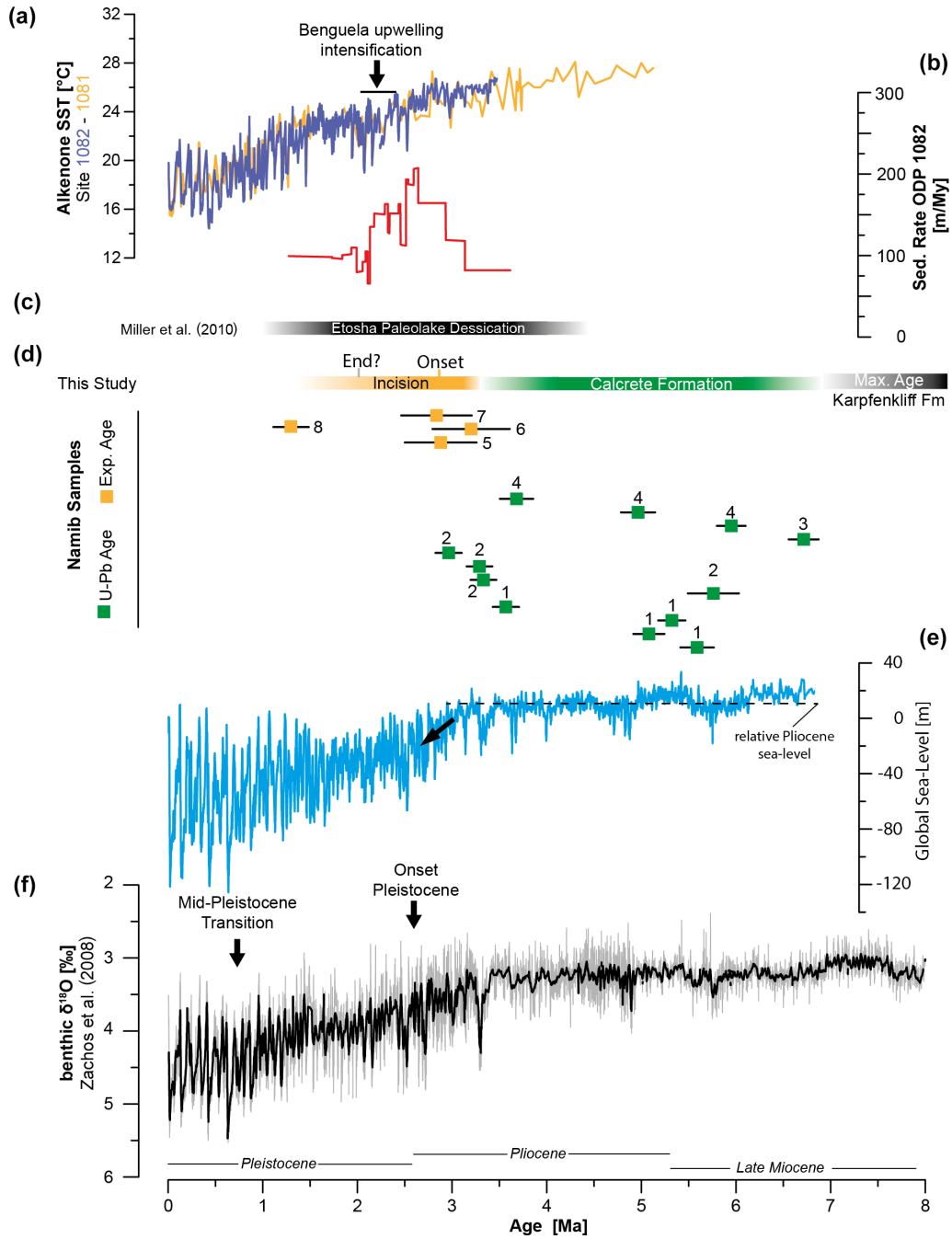


**Figure 6.** Compilation of paleoclimate records. (a) Alkenone SSTs from ODP 1082 (Etourneau et al., 2009) and ODP 1081 (Rosell-Melé et al., 2014). Intensification of Benguela upwelling according to Etourneau et al. (2009). (b) Sedimentation rate of ODP 1082 for the Pliocene–Pleistocene transitions (Dupont, 2006). (c) Desiccation of the Etosha paleolake from Miller et al. (2010). (d) U–Pb silcrete and surface exposure ages (this study). Numbers indicate identical clasts: (1) DWA98008-Silc3, (2) DWA98008-Silc4, (3) DWA98008-Silc7, (4) DWA98008-Silc8, (5) DWA98013, (6) DWA98007, (7) DWA98006, (8) DWA98024. (e) Global sea level curve from Hansen et al. (2013). Dashed black line indicates relative mean sea level during the Pliocene, followed by the global decrease since the Pliocene–Pleistocene transition. (f) Global Cenozoic reference benthic foraminifer oxygen isotope dataset (CENOGRID) from Westerhold et al. (2020).

age constraints on some sediments from the central Namib Desert, some of which are used as marker horizons throughout the region. Our chronology of groundwater calcrete formation and river incision adds crucial information with absolute dates to the “Namib Group”. Although specific precipitation ranges for calcrete formation are still being debated, we can assign potential precipitation ranges and their shifts to specific time episodes and thus provide a semi-quantitative picture of the aridification of the central Namib Desert during the Late Miocene to the Pliocene–Pleistocene. Our terrestrial paleoclimate record of microscale silcrete formation, i.e. calcrete formation, supports the marine evidence for a persistently stable Pliocene climate in the central Namib Desert. The cessation of groundwater calcrete formation was caused by the deep incision of the Kuiseb River (presumably synchronous with other E–W-flowing drainage systems of the central Namib Desert) at the Pliocene–Pleistocene transition, which can be explained by the intensification of aridity, vegetation change, and presumably global sea level drop. Global climate change with the onset of the Pleistocene was most likely the major forcing factor for major landscape rejuvenation and change in the central Namib Desert. Precipitation decline in the Kuiseb River catchment is identified as the tipping point for the local climate and landscape response.

**Data availability.** All data generated or analysed during this study are included in this published article (and its Supplement).

**Supplement.** The supplement related to this article is available online at: <https://doi.org/10.5194/gchron-5-433-2023-supplement>.

**Author contributions.** BR: fieldwork, sample preparation,  $^{21}\text{Ne}$  noble gas analysis, data evaluation, manuscript writing. RA: U–Pb dating, sample analysis thin section, Raman, data analysis, manuscript writing. AR: Raman, FMvdW: fieldwork, TJD: fieldwork, data evaluation. AG: data analysis. All authors reviewed the manuscript.

**Competing interests.** The contact author has declared that none of the authors has any competing interests.

**Disclaimer.** Publisher’s note: Copernicus Publications remains neutral with regard to jurisdictional claims made in the text, published maps, institutional affiliations, or any other geographical representation in this paper. While Copernicus Publications makes every effort to include appropriate place names, the final responsibility lies with the authors.

**Acknowledgements.** We want to thank our colleagues from the Gobabeb Research Station for their help during fieldwork in

2018. Moreover, we want to thank our preparation workshops for preparation of thin sections and pucks. We also want to thank Alan B. Woodland for his support with Raman spectroscopy. We want to thank the two anonymous reviewers for the time and effort they took to review the manuscript. This project is affiliated with the Collaborative Research Center (CRC) 1211, funded by the German Science Foundation (DFG, project no. 268236062). This is FIERCE contribution number 145.

**Financial support.** This research has been supported by the Deutsche Forschungsgemeinschaft (grant no. 268236062).

**Review statement.** This paper was edited by Daniela Rubatto and reviewed by two anonymous referees.

## References

- Allen, J.: Richards K. (ed.) 1987. *River Channels, Environment and Process*, vi 393 pp. Oxford, New York: Basil Blackwell, Price 39.50 (hard covers), ISBN 0 631 14577 X, *Geological Magazine*, 126, 313–314, <https://doi.org/10.1017/S0016756800022536>, 1989.
- Alonso-Zarza, A. M.: Palaeoenvironmental significance of palustrine carbonates and calcretes in the geological record, *Earth-Sci. Rev.*, 60, 261–298, 2003.
- Alonso-Zarza, A. M. and Wright, V.: Calcretes, *Developments in Sedimentology*, 61, 225–267, 2010.
- Balco, G., Stone, J. O., Lifton, N. A., and Dunai, T. J.: A complete and easily accessible means of calculating surface exposure ages or erosion rates from  $^{10}\text{Be}$  and  $^{26}\text{Al}$  measurements, *Quat. Geochronol.*, 3, 174–195, <https://doi.org/10.1016/j.quageo.2007.12.001>, 2008.
- Bierman, P. R. and Caffee, M.: Slow rates of rock surface erosion and sediment production across the Namib Desert and escarpment, southern Africa, *Am. J. Sci.*, 301, 326–358, 2001.
- Bonnet, S. and Crave, A.: Landscape response to climate change: Insights from experimental modeling and implications for tectonic versus climatic uplift of topography, *Geology*, 31, 123–126, 2003.
- Branca, M., Masi, U., and Voltaggio, M.: An unsuccessful attempt at U/Th dating of soil calcretes from the Doukkali area (western Morocco) and environmental implications, *Geochemistry*, 65, 347–356, 2005.
- Butt, C., Horwitz, R., and Mann, A.: Uranium occurrences in calcrete and associated sediments in Western Australia, Commonwealth Scientific and Industrial Research Organization, Report Number CSIRO-FP-16, 1977.
- Candy, I. and Black, S.: The timing of Quaternary calcrete development in semi-arid southeast Spain: investigating the role of climate on calcrete genesis, *Sediment. Geol.*, 218, 6–15, 2009.
- Candy, I., Black, S., and Sellwood, B. W.: Quantifying time scales of pedogenic calcrete formation using U-series disequilibria, *Sediment. Geol.*, 170, 177–187, <https://doi.org/10.1016/j.sedgeo.2004.07.003>, 2004.

- Cooper, F. J., Adams, B., Blundy, J., Farley, K., McKeon, R., and Ruggiero, A.: Aridity-induced Miocene canyon incision in the Central Andes, *Geology*, 44, 675–678, 2016.
- Dupont, L. M.: Late Pliocene vegetation and climate in Namibia (southern Africa) derived from palynology of ODP site 1082, *Geochem. Geophys. Geosyst.*, 7, Q05007, <https://doi.org/10.1029/2005GC001208>, 2006.
- Dupont, L. M., Donner, B., Vidal, L., Pérez, E. M., and Wefer, G.: Linking desert evolution and coastal upwelling: Pliocene climate change in Namibia, *Geology*, 33, 461–464, 2005.
- Dupont, L. M., Rommerskirchen, F., Mollenhauer, G., and Schefuß, E.: Miocene to Pliocene changes in South African hydrology and vegetation in relation to the expansion of  $C_4$  plants, *Earth Planet. Sc. Lett.*, 375, 408–417, 2013.
- Etourneau, J., Martinez, P., Blanz, T., and Schneider, R.: Pliocene–Pleistocene variability of upwelling activity, productivity, and nutrient cycling in the Benguela region, *Geology*, 37, 871–874, 2009.
- Geological Survey of Namibia: Geological map 2314 Kuiseb 1 : 250 000 ESRI Shapefile, Geological Survey of Namibia, Windhoek, Geological Series, Geological Survey of Namibia, 2016.
- Gerdes, A. and Zeh, A.: Combined U-Pb and Hf isotope LA-(MC-) ICP-MS analyses of detrital zircons: comparison with SHRIMP and new constraints for the provenance and age of an Armorican metasediment in Central Germany, *Earth Planet. Sc. Lett.*, 249, 47–61, 2006.
- Gerdes, A. and Zeh, A.: Zircon formation versus zircon alteration – new insights from combined U-Pb and Lu–Hf in-situ LA-ICP-MS analyses, and consequences for the interpretation of Archean zircon from the Central Zone of the Limpopo Belt, *Chem. Geol.*, 261, 230–243, 2009.
- Geyh, M. A. and Eitel, B.: Radiometric dating of young and old calcrete, *Radiocarbon*, 40, 795–802, 1997.
- Goudie, A.: Duricrusts in tropical and subtropical landscapes, *Duricrusts in Tropical and Subtropical Landscapes*, ISBN-10 0198232128, ISBN-13 978-0198232124, 1973.
- Goudie, A.: Calcrete, Chemical Sediments and Geomorphology: precipitates and residua in the near-surface environment, 1983.
- Goudie, A.: Organic agency in calcrete development, *J. Arid Environ.*, 32, 103–110, 1996.
- Goudie, A.: Duricrusts and landforms, in: *Geomorphology and soils*, Routledge, 37–57, 2020.
- Goudie, A. and Viles, H.: *Landscapes and landforms of Namibia*, Springer, ISBN 109402400311, ISBN 13978-9402400311, 2014.
- Goudie, A., Viles, H., Goudie, A., and Viles, H.: Calcretes: The Kamberg Calcrete Formation and the Karpencliff Conglomerate, *Landscapes and Landforms of Namibia*, 111–114, 2015.
- Hansen, J., Sato, M., Russell, G., and Kharecha, P.: Climate sensitivity, sea level and atmospheric carbon dioxide, *Philosophical Transactions of the Royal Society A: Mathematical, Phys. Eng. Sci.*, 371, 20120294, <https://doi.org/10.1098/rsta.2012.0294>, 2013.
- Herman, F. and Champagnac, J. D.: Plio-Pleistocene increase of erosion rates in mountain belts in response to climate change, *Terra Nova*, 28, 2–10, 2016.
- Herman, F., Seward, D., Valla, P. G., Carter, A., Kohn, B., Willett, S. D., and Ehlers, T. A.: Worldwide acceleration of mountain erosion under a cooling climate, *Nature*, 504, 423–426, 2013.
- Hoetzel, S., Dupont, L. M., and Wefer, G.: Miocene–Pliocene vegetation change in south-western Africa (ODP Site 1081, offshore Namibia), *Palaeogeography, Palaeoclimatology, Palaeoecology*, 423, 102–108, 2015.
- Hoetzel, S., Dupont, L. M., Marret, F., Jung, G., and Wefer, G.: Steps in the intensification of Benguela upwelling over the Walvis Ridge during Miocene and Pliocene, *Int. J. Earth Sci.*, 106, 171–183, 2017.
- Horstwood, M. S., Košler, J., Gehrels, G., Jackson, S. E., McLean, N. M., Paton, C., Pearson, N. J., Sircombe, K., Sylvester, P., and Vermeesch, P.: Community-derived standards for LA-ICP-MS U-(Th-) Pb geochronology—Uncertainty propagation, age interpretation and data reporting, *Geostand. Geoanal. Res.*, 40, 311–332, 2016.
- Houben, G. J., Kaufhold, S., Miller, R. M., Lohe, C., Hinderer, M., Noll, M., Hornung, J., Joseph, R., Gerdes, A., and Sitnikova, M.: Stacked megafans of the Kalahari Basin as archives of paleogeography, river capture, and Cenozoic paleoclimate of south-western Africa, *J. Sediment. Res.*, 90, 980–1010, 2020.
- Jacobson, P. J., Jacobson, K. M., and Seely, M. K.: Ephemeral rivers and their catchments: Sustaining people and development in Namibia, Desert Research Foundation of Namibia, Windhoek, 160 pp., 1995.
- Kelly, M., Black, S., and Rowan, J.: A calcrete-based U/Th chronology for landform evolution in the Sorbas basin, southeast Spain, *Quat. Sci. Rev.*, 19, 995–1010, 2000.
- King, L.: The geomorphology of the Eastern and Southern districts of Southern Rhodesia, *S. Afr. J. Geol.*, 54, 33–64, 1951.
- King, L. C.: Pediplanation and isostasy: an example from South Africa, *Quart. J. Geol. Soc.*, 111, 353–359, 1955.
- Korn, H. and Martin, H.: The Pleistocene in South West Africa, *Proceedings of the 3rd Pan-African Congress on Prehistory*, 14–22, 1957.
- Lancaster, N.: Paleoenvironments in the Tsondab valley, Central Namib desert, in: *Palaeoecology of Africa and of the Surrounding Islands and Antarctica*, edited by: Coetzee, J. A. and van Zinderen Bakker, E. M., Balkema, Cape Town, 411–419, 1984.
- Lifton, N., Sato, T., and Dunai, T. J.: Scaling in situ cosmogenic nuclide production rates using analytical approximations to atmospheric cosmic-ray fluxes, *Earth Planet. Sc. Lett.*, 386, 149–160, <https://doi.org/10.1016/j.epsl.2013.10.052>, 2014.
- Ludwig, K. R.: *User's Manual for Isoplot 3.75*, Berkeley Geochronological Center Special Publication No. 5., 2012.
- Mack, G. H. and James, W.: Paleoclimate and the global distribution of paleosols, *J. Geol.*, 102, 360–366, 1994.
- Maher, K., Wooden, J., Paces, J., and Miller, D.:  $^{230}\text{Th}$ -U dating of surficial deposits using the ion microprobe (SHRIMP-RG): A microstratigraphic perspective, *Quat. Int.*, 166, 15–28, 2007.
- Mann, A. and Horwitz, R.: Groundwater calcrete deposits in Australia some observations from Western Australia, *J. Geol. Soc. Austr.*, 26, 293–303, 1979.
- Marlow, J. R., Lange, C. B., Wefer, G., and Rosell-Melé, A.: Upwelling intensification as part of the Pliocene–Pleistocene climate transition, *Science*, 290, 2288–2291, 2000.
- McBride, E. F.: Quartz cement in sandstones: a review, *Earth-Sci. Rev.*, 26, 69–112, 1989.
- Miller, R.: *The Geology of Namibia*, Ministry of Mines and Energy – Geological Survey Namibia, 3, 25–21, 2008.

- Miller, R. M., Pickford, M., and Senut, B.: The geology, palaeontology and evolution of the Etosha Pan, Namibia: Implications for terminal Kalahari deposition, *S. Afr. J. Geol.*, 113, 307–334, 2010.
- Miller, R. M., Krapf, C., Hoey, T., Fitchett, J., Nguno, A.-K., Muyambas, R., Ndeutepo, A., Medialdea, A., Whitehead, A., and Stengel, I.: A sedimentological record of fluvial-aeolian interactions and climate variability in the hyperarid northern Namib Desert, Namibia, *S. Afr. J. Geol.*, 124, 575–610, 2021.
- Milnes, A. and Thiry, M.: Silcretes, in: *Developments in earth surface processes*, Elsevier, 349–377, 1992.
- Milnes, A., Wright, M., and Thiry, M.: Silica accumulations in saprolites and soils in South Australia, Occurrence, characteristics, and genesis of carbonate, gypsum, and silica accumulations in soils, *Soil Sci. Soc. Am.*, 26, 121–149, 1991.
- Molnar, P.: Climate change, flooding in arid environments, and erosion rates, *Geology*, 29, 1071–1074, 2001.
- Nash, D. J. and Shaw, P. A.: Silica and carbonate relationships in silcrete-calcrete intergrade duricrusts from the Kalahari of Botswana and Namibia, *J. Afr. Earth Sci.*, 27, 11–25, 1998.
- Nash, D. J. and Smith, R. F.: Multiple calcrete profiles in the Tabernas Basin, southeast Spain: their origins and geomorphic implications, *Earth Surf. Proc. Land.*, 23, 1009–1029, 1998.
- Netterberg, F.: The interpretation of some basic calcrete types, *S. Afr. Archaeol. Bull.*, 24, 117–122, 1969.
- Neymark, L.: Potential effects of alpha-recoil on uranium-series dating of calcrete, *Chem. Geol.*, 282, 98–112, 2011.
- Neymark, L.: Uranium–Lead Dating, Opal, edited by: Rink, W., Thompson, J., *Encyclopedia of Scientific Dating Methods*, Springer, Dordrecht, [https://doi.org/10.1007/978-94-007-6326-5\\_263-1](https://doi.org/10.1007/978-94-007-6326-5_263-1), 2014.
- Ollier, C.: Outline geological and geomorphic history of the central Namib Desert, Madoqua, 1977, 207–212, 1977.
- Oster, J. L., Kitajima, K., Valley, J. W., Rogers, B., and Maher, K.: An evaluation of paired  $\delta^{18}\text{O}$  and ( $^{234}\text{U} / ^{238}\text{U}$ ) in opal as a tool for paleoclimate reconstruction in semi-arid environments, *Chem. Geol.*, 449, 236–252, 2017.
- Partridge, T. and Maud, R.: Geomorphic evolution of southern Africa since the Mesozoic, *S. Afr. J. Geol.*, 90, 179–208, 1987.
- Pickford, M. and Senut, B.: Geology and Palaeobiology of the Central and Southern Namib Desert, Southwestern Africa: Geology and History of Study, Geological Survey, 1–155, 2000.
- Pickford, M., Senut, B., and Dauphin, Y.: Biostratigraphy of the Tsondab sandstone (Namibia) based on gigantic avian eggshells, *Geobios*, 28, 85–98, 1995.
- Pickford, M., Senut, B., Gommery, D., Andrews, P., and Banham, P.: Sexual dimorphism in *Morotopithecus bishopi*, an early Middle Miocene hominoid from Uganda, Late Cenozoic environments and hominid evolution: a tribute to Bill Bishop, 27–38, 1999.
- Rasbury, E. T. and Cole, J. M.: Directly dating geologic events: U-Pb dating of carbonates, *Rev. Geophys.*, 47, RG3001, <https://doi.org/10.1029/2007RG000246>, 2009.
- Repka, J. L., Anderson, R. S., and Finkel, R. C.: Cosmogenic dating of fluvial terraces, Fremont River, Utah, *Earth Planet. Sc. Lett.*, 152, 59–73, [https://doi.org/10.1016/S0012-821X\(97\)00149-0](https://doi.org/10.1016/S0012-821X(97)00149-0), 1997.
- Retallack, G. J.: The environmental factor approach to the interpretation of paleosols, *Factors of soil formation: A fiftieth anniversary retrospective*, Soil Science Society of America Special Publications, 33, 31–64, 1994.
- Ritter, B., Vogt, A., and Dunai, T. J.: Technical Note: Noble gas extraction procedure and performance of the Cologne Helix MC Plus multi-collector noble gas mass spectrometer for cosmogenic neon isotope analysis, *Geochronology*, 3, 421–431, <https://doi.org/10.5194/gchron-3-421-2021>, 2021.
- Rosell-Melé, A., Martínez-García, A., and McClymont, E. L.: Persistent warmth across the Benguela upwelling system during the Pliocene epoch, *Earth Planet. Sc. Lett.*, 386, 10–20, 2014.
- Ruggieri, E., Herbert, T., Lawrence, K. T., and Lawrence, C. E.: Change point method for detecting regime shifts in paleoclimatic time series: application to  $\delta^{18}\text{O}$  time series of the Pliocene–Pleistocene, *Paleoceanography*, 24, 2009.
- Rutter, E.: Pressure solution in nature, theory and experiment, *J. Geol. Soc.*, 140, 725–740, 1983.
- Scardia, G., Parenti, F., Miggins, D. P., Gerdes, A., Araujo, A. G., and Neves, W. A.: Chronologic constraints on hominin dispersal outside Africa since 2.48 Ma from the Zarqa Valley, Jordan, *Quat. Sci. Rev.*, 219, 1–19, 2019.
- Senut, B.: Fossil ratite eggshells: a useful tool for Cainozoic biostratigraphy in Namibia, *Communications of the geological Survey of Namibia*, 12, 367–373, 2000.
- Sorby, H. C.: The Bakerian Lecture: On the Direct Correlation of Mechanical and Chemical Forces, *P. R. Soc. London*, 12, 538–550, 1863.
- Stacey, J. T. and Kramers, J.: Approximation of terrestrial lead isotope evolution by a two-stage model, *Earth Planet. Sc. Lett.*, 26, 207–221, 1975.
- Stokes, M., Nash, D. J., and Harvey, A. M.: Calcrete “fossilisation” of alluvial fans in SE Spain: The roles of groundwater, pedogenic processes and fan dynamics in calcrete development, *Geomorphology*, 85, 63–84, 2007.
- Stollhofen, H., Stanistreet, I. G., von Hagke, C., and Nguno, A.: Pliocene–Pleistocene climate change, sea level and uplift history recorded by the Horingbaai fan-delta, NW Namibia, *Sediment. Geol.*, 309, 15–32, 2014.
- Stone, A.: Age and dynamics of the Namib Sand Sea: A review of chronological evidence and possible landscape development models, *J. Afr. Earth Sci.*, 82, 70–87, 2013.
- Summerfield, M.: Silcrete as a palaeoclimatic indicator: evidence from southern Africa, *Palaeogeogr. Palaeoclimatol.*, 41, 65–79, 1983a.
- Summerfield, M. A.: Petrography and diagenesis of silcrete from the Kalahari Basin and Cape coastal zone, Southern Africa, *J. Sediment. Res.*, 53, 895–909, 1983b.
- Taylor, G. and Eggleton, R.: Silcrete: an Australian perspective, *Australian Journal of Earth Sciences*, 64, 987–1016, 2017.
- Tera, F. and Wasserburg, G.: U-Th-Pb systematics in lunar highland samples from the Luna 20 and Apollo 16 missions, *Earth Planet. Sc. Lett.*, 17, 36–51, 1972.
- Van der Wateren, F. M. and Dunai, T. J.: Late Neogene passive margin denudation history – cosmogenic isotope measurements from the central Namib desert, *Global Planet. Change*, 30, 271–307, [https://doi.org/10.1016/S0921-8181\(01\)00104-7](https://doi.org/10.1016/S0921-8181(01)00104-7), 2001.
- Vermeesch, P., Fenton, C., Kober, F., Wiggs, G., Bristow, C. S., and Xu, S.: Sand residence times of one million years in the Namib Sand Sea from cosmogenic nuclides, *Nat. Geosci.*, 3, 862–865, 2010.

- Vermeesch, P., Balco, G., Blard, P. H., Dunai, T. J., Kober, F., Niedermann, S., Shuster, D. L., Strasky, S., Stuart, F. M., Wieler, R., and Zimmermann, L.: Interlaboratory comparison of cosmogenic  $^{21}\text{Ne}$  in quartz, *Quat. Geochronol.*, 26, 20–28, <https://doi.org/10.1016/j.quageo.2012.11.009>, 2015.
- Ward, J. and Corbett, I.: Towards an age for the Namib, *Namib Ecol.*, 25, 17–26, 1990.
- Ward, J. D.: The Cenozoic succession in the Kuiseb valley, central Namib desert, Geological Survey of Namibia Memoir, Windhoek, 124 p., 1987.
- Ward, J. D., Seely, M. K., and Lancaster, N.: On the antiquity of the Namib, *S. Afr. J. Sci.*, 79, 175–183, 1983.
- Weissel, J. K. and Seidl, M. A.: Inland propagation of erosional escarpments and river profile evolution across the southeast Australian passive continental margin, *Geophysical Monograph-American Geophysical Union*, 107, 189–206, 1998.
- Wendt, I. and Carl, C.: U / Pb dating of discordant 0.1 Ma old secondary U minerals, *Earth Planet. Sc. Lett.*, 73, 278–284, 1985.
- Westerhold, T., Marwan, N., Drury, A. J., Liebrand, D., Agnini, C., Anagnostou, E., Barnet, J. S., Bohaty, S. M., De Vleeschouwer, D., and Florindo, F.: An astronomically dated record of Earth's climate and its predictability over the last 66 million years, *Science*, 369, 1383–1387, 2020.
- Whipple, K. X. and Tucker, G. E.: Dynamics of the stream-power river incision model: Implications for height limits of mountain ranges, landscape response timescales, and research needs, *J. Geophys. Res.-Sol. Ea.*, 104, 17661–17674, 1999.
- Wilson, M. J.: Dissolution and formation of quartz in soil environments: A review, *Soil Sci. Annu.*, 71, 3–14, 2020.
- Yaalon, D. H. and Ward, J. D.: Observations on calcrete and recent calcic horizons in relation to landforms, central Namib desert, in: *Palaeoecology of Africa and of the Surrounding Islands and Antarctica*, edited by: Coetzee, J. A. and van Zinderen Bakker, E. M., Balkema, Cape Town, 183–186, 1982.